PNAS RESEARCH ARTICLE | NEUROSCIENCE OPEN ACCESS

Re-formation of synaptic connectivity in dissociated human stem cell-derived retinal organoid cultures

Allison L. Ludwig[a,b,c,1], Steven J. Mayerl[b,c,d,1], Yu Gao[b,e], Mark Banghart[f], Cole Bacig[b], Maria A. Fernandez Zepeda[b], Xinyu Zhao[b,c,e], and David M. Gamm[a,b,c,d,f,2]

Edited by John G. Flannery, University of California Berkeley, Berkeley, CA; received August 5, 2022; accepted December 1, 2022 by Editorial Board Member Martin S. Banks

Human pluripotent stem cell (hPSC)-derived retinal organoids (ROs) can efficiently and reproducibly generate retinal neurons that have potential for use in cell replacement strategies [Capowski *et al.*, *Development* 146, dev171686 (2019)]. The ability of these lab-grown retinal neurons to form new synaptic connections after dissociation from ROs is key to building confidence in their capacity to restore visual function. However, direct evidence of reestablishment of retinal neuron connectivity via synaptic tracing has not been reported to date. The present study employs an in vitro, rabies virus-based, monosynaptic retrograde tracing assay [Wickersham *et al.*, *Neuron* 53, 639–647 (2007); Sun *et al.*, *Mol. Neurodegener.* 14, 8 (2019)] to identify de novo synaptic connections among early retinal cell types following RO dissociation. A reproducible, high-throughput approach for labeling and quantifying traced retinal cell types was developed. Photoreceptors and retinal ganglion cells—the primary neurons of interest for retinal cell replacement—were the two major contributing populations among the traced presynaptic cells. This system provides a platform for assessing synaptic connections in cultured retinal neurons and sets the stage for future cell replacement studies aimed at characterizing or enhancing synaptogenesis. Used in this manner, in vitro synaptic tracing is envisioned to complement traditional preclinical animal model testing, which is limited by evolutionary incompatibilities in synaptic machinery inherent to human xenografts.

synapses | trans-synaptic tracing | retinal organoid | human pluripotent stem cells | photoreceptors

Significance

Synaptic contacts between neurons are required for the proper functioning of retinal and other neural circuits. Recently, the presence of functional synapses within intact human pluripotent stem cell (hPSC)-derived retinal organoids (ROs) was indirectly shown via calcium imaging. However, direct evidence supporting the capacity for de novo synaptic transmission after dissociation and re-association of retinal organoids is lacking. Since formation of synaptic connections is a necessary step in the functional replacement of retinal neurons, we employed a highly controlled, rabies virus-based monosynaptic tracing assay to investigate neuronal reconnection following dissociation of early RO cultures. Our results provide evidence for synaptic plasticity of RO-derived retinal neurons, which further establishes their theoretical potential to restore visual circuits.

Cajal's first observation of microscopic gaps between neurons more than a century ago (1) led to our current understanding of synaptic connections, which are required to establish the circuitry of the central nervous system (CNS), including the neural retina. Within the retina, two plexiform layers of synapses sequentially relay neurosensory signals from photoreceptors to retinal interneurons to retinal ganglion cells (RGCs). The first—the outer plexiform layer (OPL)—contains specialized glutamatergic synapses between light-sensitive photoreceptors (rods and cones) and interneurons (bipolar and horizontal cells, BPCs and HCs). The inner plexiform layer (IPL) comprises a network of synaptic connections between interneurons (BPCs, HCs, and amacrine cells, ACs) and retinal output RGCs.

Changes in the OPL are an early indicator of retinal degenerative diseases (RDDs) (2), and synaptic disassembly precedes the widespread neuronal death that defines the end stages of RDDs such as retinitis pigmentosa (3) and glaucoma (4), which target photoreceptors and RGCs, respectively. Periods of cellular and synaptic remodeling exist during photoreceptor and RGC (5) degenerations, suggesting the potential for tissue plasticity, but mammalian retinas are incapable of regenerating neurons once they have been lost in the course of disease or injury. As such, much effort has been directed toward strategies to restore vision in late-stage disease, either by exogenous introduction of new photoreceptors (6, 7) or RGCs (8), or endogenous re-purposing of surviving cell types (9, 10). Toward this end, photoreceptor and RGC regeneration are the focal point of the multiyear Audacious Goals Initiative of the National Eye Institute (11) and similarly focused international research activities (12). The success of these programs and all photoreceptor and RGC cell replacement therapies hinges upon the ability of human donor retinal neurons to form new synaptic contacts.

In preclinical animal model studies, human donor cells are most frequently delivered to the subretinal space as dissociated cell suspensions (5, 13–17), sheets (18–21), or whole organoids (18–20). However, all such studies require transplanted human retinal neurons to establish new synaptic connections in an evolutionarily mismatched host environment, which limits their potential to predict results in human patients. One way

This article is a PNAS Direct Submission. J.G.F. is a guest editor invited by the Editorial Board.

[1]A.L.L. and S.J.M. contributed equally to this work.

[2]To whom correspondence may be addressed. Email: dgamm@wisc.edu.

This article contains supporting information online at https://www.pnas.org/lookup/suppl/doi:10.1073/pnas.2213418120/-/DCSupplemental.

Published January 4, 2023.

to address this important limitation is to create a culture system capable of assessing whether singularized human retinal neurons can form de novo synaptic connections with each other. Ideally, the testing platform would utilize authentic retinal cell types and facilitate high-throughput analysis with rigorous controls and rapid readouts.

From a cell source perspective, human pluripotent stem cell (hPSC)-derived retinal organoids (ROs) fulfill many of the aforementioned system criteria. ROs can be produced in virtually unlimited supply, and multiple studies have confirmed the authenticity of their retinal cell progeny. More specifically, extensive evidence indicates that photoreceptors, RGCs, and other neurons differentiated within ROs exhibit hallmark histologic, physiologic, and functional characteristics of their in vivo developing counterparts (22–29), including the capacity to extend axons (30) and intrinsically respond to light in a robust and wavelength-specific manner (31). Transcriptomic studies of RO-derived neurons have revealed synaptic marker transcripts to be among the most highly expressed in both photoreceptors (29, 32, 33) and RGCs (34, 35). Likewise, protein expression studies have shown developmentally appropriate localization of synaptic proteins within the putative plexiform layer(s) of ROs (22, 23, 36–39) and along processes of cultured retinal neurons extracted from dissociated ROs (25, 40). Importantly, the synapses and circuits that develop within intact ROs were recently confirmed to be functional (23). Thus, a growing body of in vitro evidence suggests that RO-derived neurons can form bona fide functional synapses, at least within an unperturbed 3D organoid environment.

Despite xenograft limitations, modest alterations to light-evoked responses have been reported after transplantation of hPSC-RO-derived photoreceptors as single cells (5, 13, 15, 41, 42) or sectioned tissue sheets (18, 21, 43) in different animal model systems (5, 42). However, it can be difficult to determine whether such function is attributable to cell replacement with synaptic reconstruction or to indirect effects on host neurons via neuroprotective factors or biomaterial transfer (6, 19, 44, 45). Furthermore, nearly all electrophysiologic and behavioral tests that assess the outcomes of retinal neuron replacement in preclinical animal models rely on the assumption that synaptic connections with donor cells have occurred (5, 13, 15, 18, 20, 21, 41–43). Direct demonstration of the capacity for cultured photoreceptors and RGCs to re-form such connections would therefore increase confidence in their use as donor material for future clinical trials.

Synaptic tracing is a commonly used approach for studying connections between neurons within the CNS (46, 47). Monosynaptic tracing with G-glycoprotein-deleted rabies virus (RVdG) (48)—which travels retrograde across a single synapse—is widely employed for synaptic tracing studies (46) due to its low neurotoxicity in short-term culture and greater versatility relative to historically used viral tracers (49). With appropriate titration of viral transduction levels and incorporation of controls (47), monosynaptic RVdG tracing can serve as a powerful tool for studying existing and reconstructed neural circuits (50–52). In the present study, we used monosynaptic RVdG tracing to answer a simple but as yet unanswered question: do hPSC-derived retinal neurons possess intrinsic potential to form new synaptic connections after extraction from organoids? We fully dissociated and triturated ROs, passed the dissociated cell suspension through a small-pore cell strainer, and plated the resulting mixed population of retinal cell types in 96-well plates to permit subsequent unbiased analysis using automated high-content imaging. After 10 days (10 d), the 2D cultures were subjected to an established RVdG assay, which revealed robust tracing in multiple types of retinal neurons, including photoreceptors and RGCs. Combined with recent evidence showing their capacity for complex intrinsic functional responses (30, 31, 40, 53, 54), these results lend credence to the employment of human RO-derived photoreceptors and RGCs for cell replacement efforts.

Results

2D Cultures of Dissociated hPSC-ROs Contain Major Classes of Retinal Neurons and Express Synaptic Proteins. Prior to investigating whether RO-derived neurons can reconnect following dissociation, we first needed to convert 3D ROs to a 2D culture system and determine the proportion of different cell classes that remained after plating. Stage 2 (day 80, or D80) wild-type WA09 (55) hPSC-ROs were produced as previously described (22), dissociated to a single cell suspension using papain, triturated repeatedly, passed through a small-pore cell strainer, mixed, and plated onto individual wells of 96-well plates (200,000 cells/well) (Fig. 1*A*). Papain was chosen for its known devastating effect on preexisting synapses and, consequentially, its frequent use for cell dissociation in synaptic tracing studies (56–59). Day 80 of differentiation was selected because ROs contain a cross-section of neuron subpopulations at this timepoint, including RGCs, interneurons, and photoreceptors (22, 60) (Fig. 1*B*), as well as residual neural retina progenitor cells and few, if any, Müller glia (22). In addition, some retinal neurons, particularly RGCs, undergo degeneration in later-stage ROs (22). Last, photoreceptors in older ROs are less tolerant of dissociation and more expensive to manufacture clinically, all of which favors the use of earlier stages for cell replacement therapies (6, 8).

After dissociation and plating on day 80, cells were allowed to recover and extend neuronal processes for 20 d, whereupon they were fixed in paraformaldehyde and screened with a battery of antibodies against neural retina cell fate markers. Markers with consistent, reliable expression in the 2D cultures included cone-rod homeobox (CRX), recoverin (RCVN), synuclein gamma (SNCG), and calbindin (CALB). Other cell type-selective markers known to be expressed in intact ROs at this stage [calretinin (CaR), cellular retinaldehyde binding protein (CRALBP), ONECUT1, microphthalmia-associated transcription factor (MITF), and visual system homeobox 2 (VSX2)] were not detected postdissociation, either due to selective cell loss or marker downregulation. With the battery of markers available, we were able to distinguish the following broad classes of retinal cells: photoreceptors (CRX, RCVN), RGCs (SNCG), and retinal interneurons (CALB). Of note, these markers are not fully specific to each cell type when used in isolation. For example, CRX is present in all photoreceptors but is also found in immature retinal pigment epithelial (RPE) cells. However, unlike photoreceptors, RPE cells do not express RCVN. In addition to marker expression, cell morphology and proliferative status were also used to delineate general cell classes. RPE cells are large and flat and do not have defined processes, whereas RGCs display long axons and photoreceptors generally possess one or two short processes. Last, both retinal progenitor cells (RPCs) and RPE cells are highly proliferative (Ki67+), whereas all neural retina cell classes of interest are postmitotic. Based on these collective criteria, we were confident in assigning retinal neurons as either photoreceptors, RGCs, or retinal interneurons, but we were not able to reliably distinguish between subclasses of retinal interneurons (ACs, HCs, and BPCs).

After validating antibodies in the 2D system, we quantified cell populations via unbiased high-content image analysis (HCIA) (Fig. 1*C*) in accordance with previously described methods

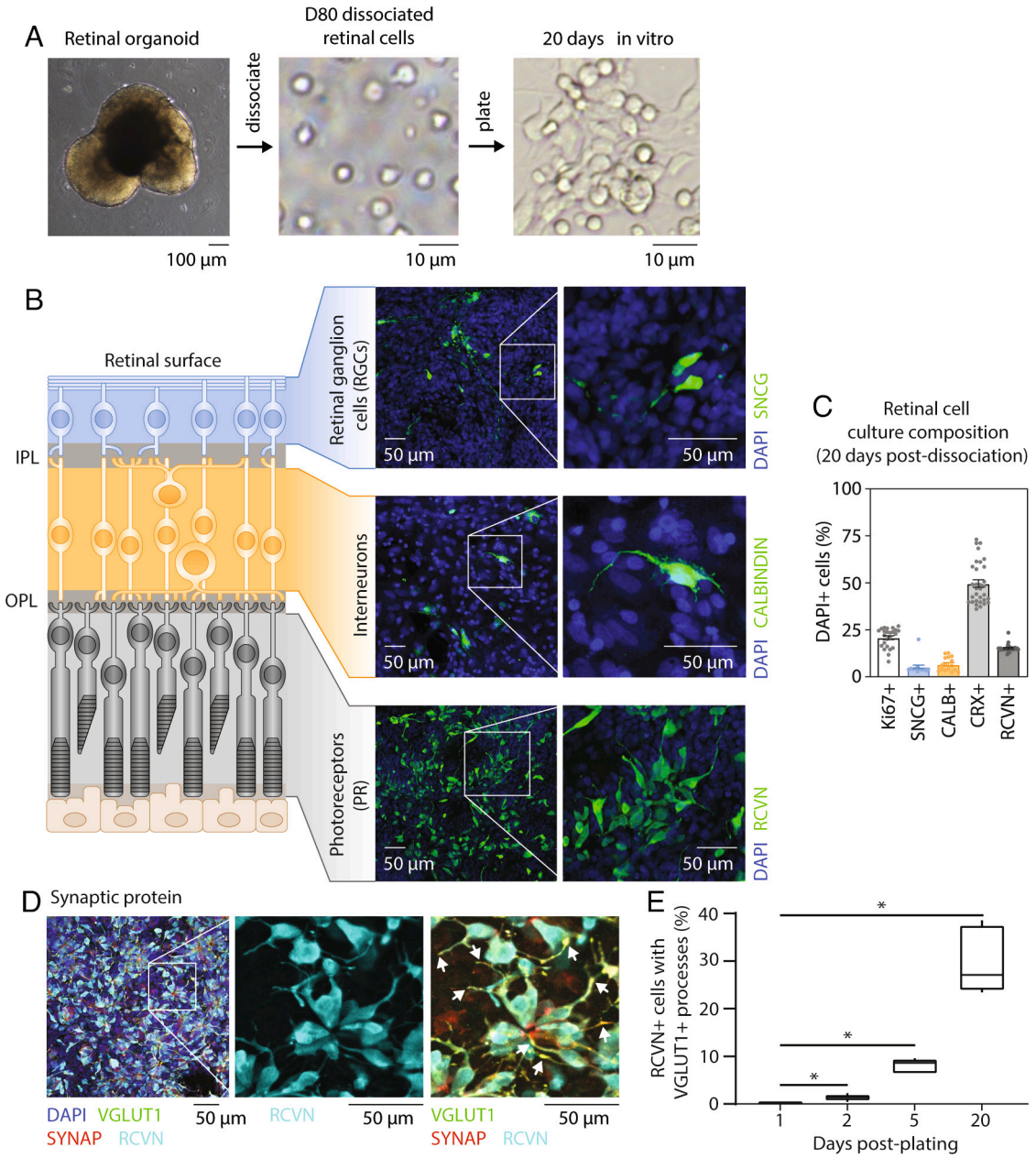

Fig. 1. Retinal neuron diversity in dissociated hPSC-derived RO cultures. (*A*) Experimental overview showing the appearance of (*Left*) an intact stage 2 RO (D89 shown), (*Middle*) retinal cells immediately following dissociation of a D80 RO, and (*Right*) dissociated retinal cells 20 d after plating. (*B*) ICC showing the relative appearance and qualitative abundance of SNCG+ (RGCs), CALB+ (retinal interneurons), and RCVN+ (maturing photoreceptors) cells in dissociated D80 RO cultures 20 d after plating, alongside a schematic depicting their location in intact retinal tissue. (*C*) Quantification of retinal cell populations expressing SNCG, CALB, RCVN, Ki67 (dividing cells, including retinal progenitors and RPE cells), and/or CRX (newborn and maturing photoreceptors) in dissociated D80 RO cultures 20 d after plating. (*D*) RCVN+ photoreceptors express the synaptic proteins VGLUT1 and SYNAP 20 d after D80 RO dissociation and plating, which colocalize with each other along photoreceptor axons (arrows). Scale bars: 100 µm, 50 µm, or 10 µm as indicated on their respective panels. (*E*) Quantification of RCVN+ cells possessing processes with VGLUT1+ puncta at day 1, 2, 5, and 20 d postplating. At day 1, RCVN+ cells (n = 467) displayed rare processes, none of which contained VGLUT1+ puncta. Thereafter, the percentage of RCVN+ cells having processes with VGLUT1+ puncta increased substantially (day 2: 1.4 ± 0.6%, n = 559 cells; day 5: 8.4 ± 1.4%, n = 633 cells; day 20: 29.5 ± 7.1%, n = 749 cells) (*$P < 0.05$, Kruskal–Wallis with pairwise Mann–Whitney *U* analyses).

(32, 61). A substantial population of Ki67+ proliferative cells (20.8 ± 1.1% of DAPI+ cells, $n = 24$ replicate wells) were observed (Fig. 1*C* and *SI Appendix*, Fig. S1*A*), representing presumptive RPE cells and RPCs (22, 60). SCNG+ RGCs (5.3 ± 1.3% of DAPI+ cells, $n = 12$ replicate wells) and CALB+ cells (6.7 ± 0.9% of DAPI+ cells, $n = 16$ replicate wells) were also detected (Fig. 1*C*). CRX+ cells—representing all photoreceptors and some RPE (32)—predominated within dissociated 2D cultures (49.6 ± 2.0% of DAPI+ cells, $n = 32$ replicate wells) (Fig. 1*C* and *SI Appendix*, Fig. S1*B*). RCVN, expressed in more mature photoreceptors (and a subset of later-born BPCs) (22), was detected in 15.2 ± 0.4% of all DAPI+ cells ($n = 26$ replicate wells) (Fig. 1 *B* and *C*). Overall, the relative proportions of broad cell classes found in 2D cultures of dissociated D80 ROs at 20 d postplating approximated that of intact D80 ROs at the time of dissociation (22, 26, 27, 32, 40).

We next examined the potential for plated retinal neurons to express synaptic markers 20 d after dissociation of D80 ROs. Consistent with recent studies using developmentally matched dissociated retinal neurons (30, 62), expression of synaptic proteins was observed in RCVN+ photoreceptor processes by day 20. More specifically, the presynaptic proteins vesicular glutamate transporter 1 (VGLUT1) and synaptophysin (SYNAP) frequently

colocalized within photoreceptor processes, forming puncta (Fig. 1*D*). To assure that any preexisting synaptic connections were abolished during dissociation, we also examined VGLUT1 localization at 1, 2, 5, and 20 d postplating. On day 1, rare photoreceptor processes were present, none of which contained VGLUT1+ puncta. This finding is in accordance with Rempel et al. (30), who showed that synaptic proteins redistribute to the cytoplasm of photoreceptor cell bodies following dissociation of ROs with papain. Thereafter, the percentage of RCVN+ photoreceptors possessing processes with VGLUT1+ puncta increased substantially ($P < 0.05$, Kruskal–Wallis with pairwise Mann–Whitney *U* analyses, n = 3-4 20X images quantified per time point), reaching 29.5 ± 7.1% of RCVN+ cells by day 20 (Fig. 1*E*). Last, we immunostained for an additional synaptic marker, excitatory amino acid transporter 3 (EAAT3) (63), and observed EAAT3+ puncta within SNCG-positive RCG neurites at day 20 (*SI Appendix*, Fig. S1*C*). Taken together, these results demonstrate the presence of three broad classes of retinal neurons in 2D plated cultures of dissociated ROs, along with concurrent expression of synaptic proteins in RGC and photoreceptor processes.

Monosynaptic Retrograde Tracing Assay Design and Validation. To determine whether RO-derived neurons could re-form synaptic connections following dissociation, we adapted a monosynaptic rabies virus tracing assay for use in the 20-day 2D culture system described above (i.e., dissociation and plating of D80 ROs with final analysis on D100) (Fig. 2). A replication-deficient rabies virus that includes an mCherry transgene (RaV-mCherry) was pseudotyped by replacing the *Rgp* gene (R), which encodes the rabies envelope glycoprotein and allows RaV to enter mammalian cells, with *EnvA*, an envelope glycoprotein-encoding gene specific to the avian sarcoma leukosis virus. EnvA-pseudotyping alters RaV tropism, eliminating its ability to infect mammalian cells and limiting its entry exclusively to cells expressing the avian sarcoma leukosis virus receptor, subgroup A (abbreviated TVA) (49, 64–67).

To facilitate controlled introduction of pseudotyped RaV-mCherry into retinal cells, we transduced plated cultures at 10 d postdissociation (D90) with a lentivirus (abbreviated lenti-GTR) expressing transgenes for the following: 1) green fluorescent protein (GFP) linked to a nuclear localization signal, 2) TVA (to enable infection with RaV-mCherry), and 3) Rgp (to permit monosynaptic retrograde RaV-mCherry transmission). 5 d later (D95), the cultures were transduced with RaV-mCherry. Only lenti-GTR-infected cells (identified by green nuclei) can take up and transmit RaV-mCherry due to their exclusive expression of TVA and Rgp, respectively. Cells that are transduced with both lenti-GTR and RaV-mCherry thus possess green nuclei and red cytoplasm and are hereon referred to as starter cells. RaV produced in starter cells is competent to traverse single synapses into connected presynaptic cells, where it subsequently directs the expression of cytoplasmic mCherry. These presynaptic cells, hereon referred to as traced cells, can be readily identified by their red cytoplasm and unlabeled nuclei (Fig. 2*A*). Since a high number of starter cells makes it difficult or impossible to reliably quantify subsequent presynaptic tracing events (64, 68), lentivirus titers were optimized to achieve sparse (≤5%) transduction (*SI Appendix*, Fig. S2).

After sequential transduction with lenti-GTR (D90) and RaV-mCherry (D95), 2D retinal cell cultures were quantitatively examined on D100 for the presence of starter and traced cells using confocal and high-content widefield imaging. In addition, all experiments included two control conditions treated at the same time points to monitor nonspecific RaV-mCherry uptake or biomaterial transfer (45, 69, 70–73). First, a negative control (RaV only at D95) was included to confirm that RaV-mCherry uptake was exclusive to starter cells transduced with lentivirus. Indeed, in the absence of lentivirus, essentially no RaV-infected cells (i.e., cells with red-labeled cytoplasm) were observed [0.02% (95% CI: 0.01, 0.04) of DAPI-positive cells, $n = 34$ replicate wells] (Fig. 2*B*). Second, to account for nonsynaptic transfer of fluorescent reporter proteins, we employed a control lentivirus lacking the *Rgp* transgene (lenti-GTΔR) (Fig. 2*C*). Lenti-GTΔR control cultures were transduced 10 d after plating (D90) and infected with RaV-mCherry on D95 as detailed above, which labels a population of starter cells (i.e., green nucleus and red cytoplasm) that is incapable of true monosynaptic RaV transfer. The median detection rate of artifactually labeled presynaptic cells (red cytoplasm only) in lenti-GTΔR controls was low [1.4% (95% CI: 1.1, 1.9) of DAPI-positive cells, $n = 37$ replicate wells], which is in line with prior reports (64, 65) and consistent with only rare instances of nonsynaptic transfer of mCherry protein.

In dissociated hPSC-RO cultures containing starter cells competent to undergo monosynaptic tracing (i.e., treated with lenti-GTR + RaV) (Fig. 2*D*), we observed a highly significant increase in the detection of labeled presynaptic cells compared to both lenti-GTΔR + RaV and RaV-only controls [6.2% (95% CI: 5.6, 6.9) of DAPI-positive cells, $n = 45$ replicate wells; $P < 0.00001$ for both comparisons using Mood's test of equal medians; see also *SI Appendix*, Fig. S3 for reproducibility across five independent differentiations]. De novo synaptic connections, as demonstrated by successful RaV-mCherry transmission, were thus readily identifiable within postdissociation retinal neuron cultures. Starter cells within lenti-GTR cultures were almost exclusively neural (*SI Appendix*, Fig. S4), with CRX- or RCVN-positive photoreceptors being the most prevalent (43.3 ± 4.5% and 44.8 ± 5.3% of all starter cells; $n = 8$ and 6 replicate wells, respectively), followed by SNCG-positive RGCs (32.2 ± 5.7%, $n = 8$ replicate wells) and CALB-positive interneurons (12.0 ± 3.2%, $n = 3$ replicate wells). A smaller proportion of starter cells (3.2 ± 0.9%, $n = 6$ replicate wells) were Ki67 positive.

Photoreceptors, Retinal Ganglion Cells, and Interneurons Contribute to Traced Cell Populations. Finally, we examined whether specific groups of retinal neurons—photoreceptors, RGCs, and interneurons—were among traced presynaptic cell populations (Fig. 3). Lenti-GTR + RaV-treated cultures were colabeled with the set of five cell type markers validated in 2D untraced cultures (Fig. 1), and unbiased HCIA was used to assess which retinal neurons, if any, were consistently identifiable among traced cells. The three major classes of hPSC-derived retinal neurons (Fig. 3*A*) were detected among traced presynaptic cells, with CRX- or RCVN-positive photoreceptors being most frequently traced (39.7 ± 4.1% or 41.1 ± 4.2% of traced neurons, respectively; $n = 8$ and $n = 10$ replicate wells, respectively) (Fig. 3*B* and *SI Appendix*, Fig. S5). RGCs were the second-most abundant, with SNCG-positive cells representing 19.0 ± 2.8% of all traced presynaptic neurons ($n = 8$ replicate wells). CALB-positive cells with interneuron-like morphology (larger soma and multiple dendrites) comprised 12.2 ± 0.6% of traced cells ($n = 4$ replicate wells). As an internal control, Ki67-positive cells (presumptive RPCs or RPE)—deemed unlikely or incapable of forming synaptic contacts—were also quantified. Relative to neuronal cells, traced Ki67-positive cells were rarely detected (4.9 ± 1.3% of traced cells; n = 6 replicate wells). The synapse formation index (SFI)—a ratio of traced to starter cells—reflects the population-level average number of traced presynaptic cells per starter cell. In lenti-GTR + RaV cultures, the SFI was 1.3, consistent with connectivity slightly greater than one to one between starter and traced cells.

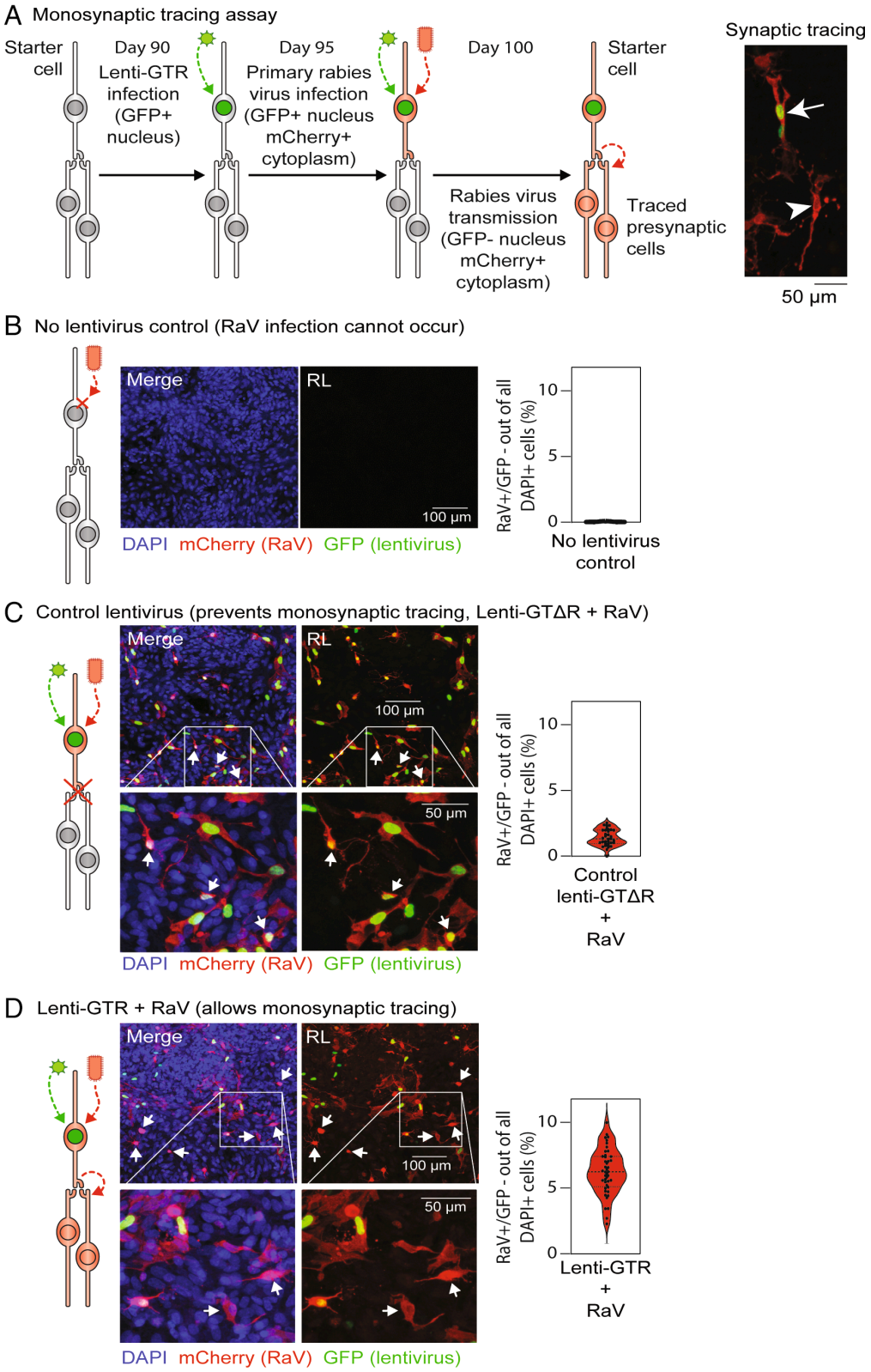

Fig. 2. Monosynaptic retrograde rabies virus tracing assay design and validation. (*A*) Schematic depicting the two-step RaV synaptic tracing assay utilized for this study, alongside a fluorescence image from one of the experiments (*Far Right*) showing an example of a starter retinal cell (arrow) and a traced presynaptic retinal cell (arrowhead). ROs were dissociated and plated on day 80 of differentiation. Resulting 2D cultures were infected with lentivirus 10 d later (day 90), followed by RaV infection at day 95 and examination for the presence of starter and traced presynaptic cells at day 100. (*B*) In the absence of primary transduction with lenti-GTR (i.e., no lentivirus control), secondary RaV infection cannot occur, resulting in negligibly detectable fluorescent cells. (*C*) Primary transduction with lenti-GTΔR followed by secondary RaV infection permits labeling of starter retinal cells (GFP+ nuclei and mCherry+ cytoplasm) (arrows) but does not allow true monosynaptic tracing. Therefore, the small fraction of cells that have GFP-negative nuclei and mCherry+ cytoplasm in these control experiments represent nonspecific biomaterial transfer (i.e., false traced presynaptic cell detection rate). (*D*) In experimental cultures, primary transduction with lenti-GTR followed by secondary RaV infection leads to labeling of both starter retinal cells and traced presynaptic retinal cells (arrows). The median percentage of traced presynaptic cells was significantly greater in lenti-GTR + RaV cultures [6.2% (95% CI: 5.6, 6.9) of DAPI+ cells, $n = 45$ replicate wells] (*D*) relative to lenti-GTΔR + RaV controls [1.4% (95% CI: 1.1, 1.9) of DAPI+ cells, $n = 37$ replicate wells] (*C*) or RaV-only controls [0.02% (95% CI: 0.01, 0.04) of DAPI+ cells, $n = 34$ replicate wells]; $P < 0.00001$ using Mood's test of equal medians. Scale bars: 100 µm, 50 µm as indicated on respective panels.

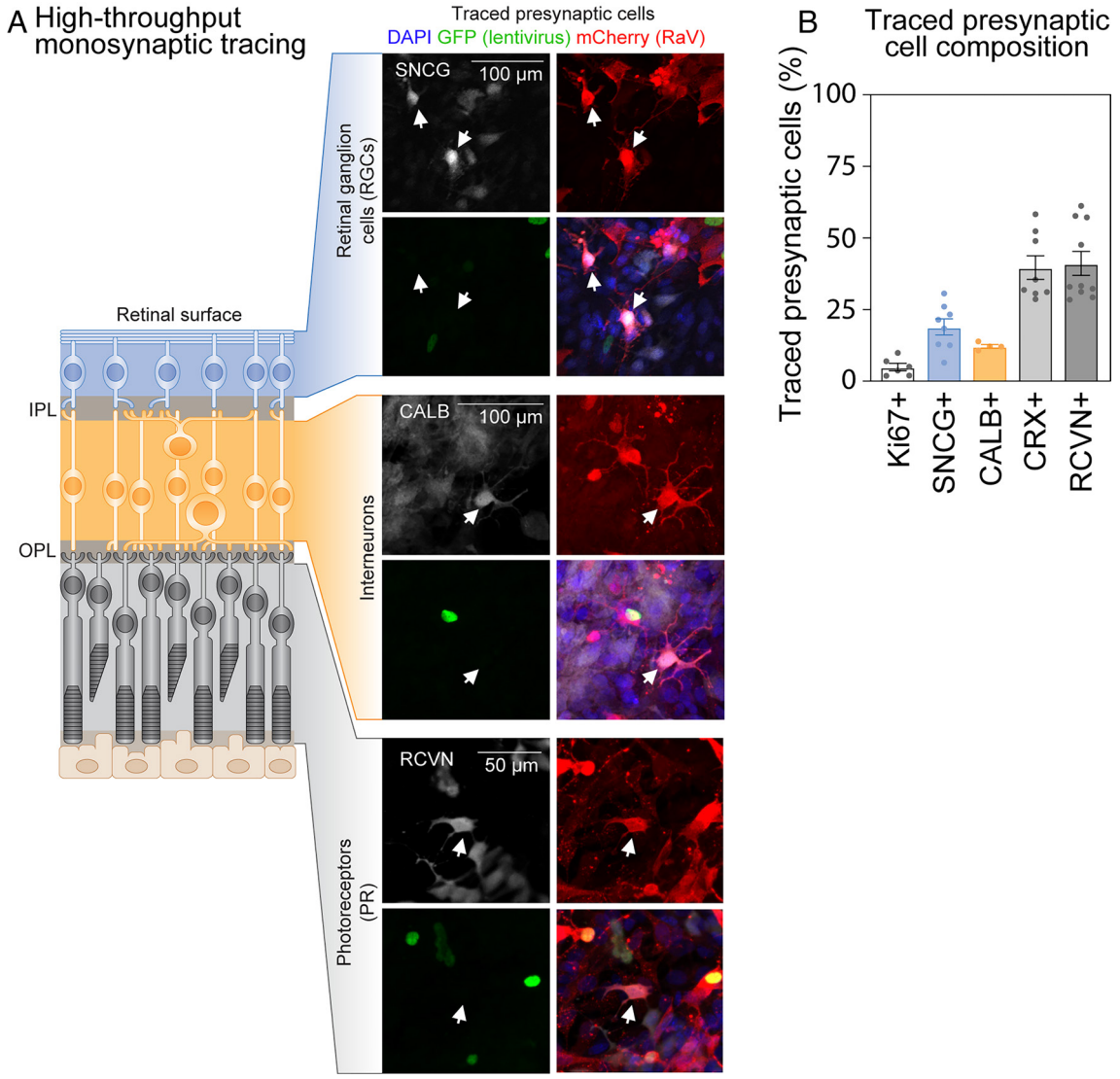

Fig. 3. Monosynaptic retrograde rabies virus tracing reveals new synaptic contacts formed by photoreceptors, interneurons, and retinal ganglion cells after dissociation from ROs. (*A*) ICC images showing representative traced presynaptic cells (arrows) alongside a schematic depicting their corresponding location within intact retinal tissue (*Top* panels: SNCG+ retinal ganglion cells; *Middle* panels: CALB+ retinal interneuron; *Lower* panels: RCVN+ photoreceptor). (*B*) Quantification of traced presynaptic cell populations coexpressing markers of proliferation (Ki67), retinal ganglion cells (SNCG), retinal interneurons (CALB), or photoreceptors (CRX, RCVN). Error bars represent SDs. Scale bars: 100 µm or 50 µm as indicated on respective panels.

Discussion

With momentum building toward human clinical trials for neuroretinal cell replacement (74, 75), there is a growing need to investigate the potential for hPSC-derived donor retinal neurons to make de novo synapses. To date, there is indirect evidence consistent with low rates of functional synaptogenesis following hPSC-photoreceptor transplantation in rodents and nonhuman primates (5, 11, 13, 14, 19, 21, 76), and even less is known about the degree of synaptogenesis occurring after hPSC-RGC transplantation (8).

In this study, we demonstrate that differentiating hPSC-derived retinal neurons—predominantly photoreceptors and RGCs—are capable of forming new synaptic connections after RO dissociation. These findings extend the work of several studies describing the synaptic structure and function of hPSC-photoreceptors and other organoid-derived retinal neurons (22, 23, 36, 40). For example, a report by Cowan et al. provided evidence of functional synapses within intact ROs, although the origin of the synaptic signals was assumed by cell location rather than by marker colocalization (23). Upon dissociation of ROs, Rempel et al. showed that immature photoreceptors extend axons for a brief period, after which there is a redistribution of synaptic markers from the cell body to the axon terminal (30). Our study further suggests that differentiating hPSC-retinal neurons, including those of particular interest for cell replacement therapies, retain the capacity to form new synapses following removal from the organoid environment.

Monosynaptic RVdG tracing facilitated a systematic, quantitative approach to studying de novo synaptic connections among hPSC-retinal neurons. Although synaptic tracing does not provide direct information regarding general synaptic maturity or function (47), our results at minimum demonstrate broad plasticity of synaptic interactions among dissociated hPSC-retinal neurons. Despite wide adoption in CNS development and transplantation research [see Saleeba et al. (46) and Adler et al. (50)], and precedent for its use in the retina (77, 78), monosynaptic RVdG tracing has not previously been applied to hPSC-retinal neurons (6). The presence of specialized ribbon synapses in photoreceptors and bipolar cells has been speculated to pose a barrier to wild-type RaV tracing in adult animals (6, 79). However, our study utilized pseudotyped RaV and hPSC-retinal neurons at a stage of maturity prior to ribbon

synapse formation, and thus circumvented this potential issue. Future studies will examine the potential for hPSC-photoreceptors to form more mature synaptic architecture in long-term cultures of dissociated ROs or cocultures with adult retinal cells. Such efforts will require significant advancements in the current 2D in vitro model system to maintain viability of postmitotic retinal neurons and avoid overgrowth of nonneuronal cell types over time.

The discovery of biomaterial transfer as a potential false indicator for integration in previous mouse studies of photoreceptor transplantation (45, 69–73) underscores the need to investigate the mechanistic underpinnings of neuroretinal cell therapies (6, 7, 44, 74, 78, 79). The synaptic tracing tools and assay methods employed herein provide a rigorous and unbiased means of assessing biomaterial transfer and other confounding variables. In addition, our system can be employed to evaluate the potential of endogenous and exogenous factors to enhance hPSC retinal neuron synaptogenesis, which in turn might improve functional outcomes after transplantation.

In summary, we have developed a quantitative and relatively high-throughput approach for identifying and quantifying de novo synaptic contacts formed by hPSC-derived retinal neurons. Given a lack of robust anterograde synaptic labeling strategies, monosynaptic retrograde RVdG tracing represents one of only a few available strategies for studying these connections. Future efforts will employ cell sorting techniques and/or different promoters to further examine the propensity of specific populations of hPSC-derived retinal neurons to form new pre- or post-synaptic connections over the course of their differentiation, and will also seek to characterize the strength and function of such synapses. In addition, the synaptic tracing tools described herein could be applied to other host model systems to address questions of functional synapse formation after allogeneic (e.g., using ex vivo human retinal tissue) or xenogeneic (e.g., using animal models) transplantation (80). Incorporation of multiple negative controls allows this assay to distinguish bona fide synaptic connections, thus providing a means to verify the mechanism behind vision recovery following intraocular delivery of donor retinal neurons.

Materials and Methods

RO Differentiation. Stage 2 (day 80 of differentiation, D80) ROs were differentiated from WA09 hPSCs (WiCell) according to a retinal differentiation protocol recently described by Capowski et al. (22). Reagents (summarized in *SI Appendix*, Table S1) and plasticware were obtained from Thermo Fisher unless otherwise indicated. hPSC colonies were maintained on Matrigel (WiCell) in StemFlex or MTesR Plus pluripotency media (STEMCELL Technologies) prior to initiating retinal differentiation. Colonies were lifted with ReLeSR passaging reagent (STEMCELL Technologies) and grown in suspension to form 3D embryoid bodies (EBs) on D0. EBs were gradually transitioned from pluripotency medium to neural induction medium [NIM; 1:1 Dulbecco's modified Eagle's medium (DMEM):F12, 1× minimum essential medium (MEM) nonessential amino acids (NEAA), 1× GlutaMAX, 2 mg/mL heparin (MilliporeSigma), and 1% N2 supplement] over 4 d followed by treatment with 0.5× bone morphogenetic protein 4 (BMP4, R&D Systems) on D6. EBs were plated onto Matrigel on D7 and maintained with periodic NIM half media changes to reduce the BMP4 concentration through D15. On D16, cultures were transitioned to retinal differentiation medium [RDM; 3:1 DMEM:F12, 1× MEM NEAA, 1× GlutaMAX, 1× antibiotic-antimycotic, and 2% B27 supplement] and maintained with thrice-weekly media changes until dissection. Near D30 of differentiation, ROs were dissected and maintained in poly-hydroxyethylmethacrylate (poly-HEMA, MilliporeSigma)-coated T25 flasks with twice-weekly 3D RDM changes [RDM +5% fetal bovine serum (WiCell), 100 μM taurine (MilliporeSigma), and 1:1,000 chemically defined lipid supplement].

Virus Production. Lenti-GTR and lenti-GTΔR were cloned using lenti-CMV-GFP vector as a backbone (66), and the CMV-GFP cassette was replaced with EF1-GFP-TVA-Rgp or EF1-GFP-TVA. The GFP-TVA-Rgp and GFP-TVA cassettes were cloned from yugao-1 (addgene plasmid #158208) and yugao-2 (addgene plasmid #158209), respectively, and confirmed via Sanger sequencing after insertion. Lentivirus production was performed as described previously (66) with modifications. Briefly, lentiviral DNA was cotransfected with the packaging plasmids pMDL, REV, and pCMV-Vsvg into HEK293T cells using the polyethylenimine (PEI) method. The viral transfer vector DNA and packaging plasmid DNA were transfected into one 15-cm dish of cultured HEK293T cells with PEI. The medium containing lentivirus was collected at 36, 60, and 84 h posttransfection, pooled, filtered through a 0.2-μm filter, and concentrated using an ultracentrifuge at 19,000 rpm for 2 h at 4 °C using a SW32Ti rotor (Beckman). The virus was washed once and then resuspended in 50 μL 1× phosphate-buffered saline (PBS). We routinely obtained 5×10^8 infectious viral particles/mL for lentivirus. Lentivirus stock solutions were diluted with sterile 1× PBS to prepare a 1:10 working solution for subsequent use.

Pseudotyped rabies viral vector was produced as previously described (65, 67). Envelope protein EnvA-pseudotyped (i.e., Rgp-null) rabies virus carrying an mCherry reporter gene was generated in a helper cell line (BHK-EnvARGCD), and RaV-mCherry stock was produced by collecting, filtering, and concentrating the supernatant. Stock titers of 10^8 viral particles/ml were routinely obtained. Rabies virus stock was diluted in a 1:5 working solution in 1× PBS prior to use.

Monosynaptic RVdG Retrograde Tracing. Stage 2 (D80) ROs were dissociated with papain (Worthington Biochemical), triturated repeatedly, passed through a 37-μm small-pore mesh cell strainer, and plated onto 96-well plates coated with poly-D-lysine (MilliporeSigma) at a density of 200,000 cells/well (6,250 cells/mm^2). Cultures were transfected with viral vectors according to methods described by Sun et al. with slight modifications (64). On D90, the cultures were transfected with lentiviral vectors (lenti-GTR working solution 0.1X in 3D RDM; lenti-GTΔR working solution 0.01X in 3D RDM) to sparsely label a population of starter neurons, avoiding oversaturation of cultures with traced presynaptic neurons. RaV-only controls were concurrently treated with 1× PBS. On D95, the cultures were treated with 1:40 RaV-mCherry working solution in 3D RDM. A full media change with fresh 3D RDM was performed 24 h after each transfection.

Immunocytochemistry (ICC). Samples were fixed in 4% paraformaldehyde for 10 min at room temperature and washed three times with 1× PBS. Fixed samples were incubated in donkey blocking solution [10% normal donkey serum (MilliporeSigma), 5% bovine serum albumin (MilliporeSigma), and 0.5% Triton-X (MilliporeSigma) in 1× PBS] for 1 h and incubated in primary antibodies (*SI Appendix*, Table S2) overnight at 4 °C. Following primary antibody incubation, the samples were washed with 1× PBS and incubated for 35 min in the dark at room temperature in secondary antibody solution with 4′6-diamidino-2-phenylindole (DAPI) and species-specific secondary antibodies (Alexa Fluor 488, 546, and 647) diluted at 1:500. The samples were washed with 1× PBS and stored in light-protective containers at 4 °C until imaging. ICC for postdissociation synaptic puncta time course experiments was conducted identically, and cells were fixed with 4% paraformaldehyde 1, 2, 5, or 20 d after dissociation (days 81, 82, 85, or 100 of differentiation, respectively).

HCIA. Immunostained 96-well plate samples from five independent hPSC-RO differentiations were subjected to HCIA as previously described by Phillips et al. with minor modifications (32). Briefly, 23 fields were captured per well (*SI Appendix*, Fig. S6) at 20× magnification with a high-content wide-field imaging system (Operetta, PerkinElmer). Segmentation and analysis were performed on unprocessed images using Columbus software (PerkinElmer). Border objects and pyknotic nuclei (determined by size and DAPI intensity) were programmed to be excluded from quantitative analyses. Cells positive for each marker were identified by scatter plot gating of fluorescence intensity for standardized segmentation and analysis workflows. For consistency in gating and marker analysis, data from all five replicates were used to develop each HCIA workflow. Cell counts from all 23 image fields for a single well were summed for a single biological replicate (on average, approximately 25,000 cells/well) for quantitative analyses; reported *n* values are equivalent to the number of wells included.

Statistics. Descriptive statistics were performed with and visualized in GraphPad Prism. Central tendency was reported as the mean ± SE unless otherwise specified in the text. Statistical analyses for assay validation were performed in R version 4.0.0 (R Core Team, 2020) using packages described in *SI Appendix*,

Table S3. Where referenced, median values and a 95% CI were determined using the exact method.

Data, Materials, and Software Availability. Cell counts and R code data have been deposited in Mendeley Data (10.17632/ncmn2msdhx.1) (81). All other data are included in the article and/or *SI Appendix*.

ACKNOWLEDGMENTS. We thank Dr. Rick Chappell (UW-Madison Dept. of Statistics) for statistical consultation and analysis, Dr. Karla Knobel (Waisman Center Cellular Imaging and Analysis Core) for high-content imaging consultation, Dr. Edward Callaway (Salk Institute) for providing pseudotyped rabies virus stock, and H. Adam Steinberg (Artforscience.com) for graphical consultation. Further, we wish to acknowledge Dr. Donald Zack, Dr. Timothy Gomez, and members of the Gamm lab for thoughtful discussion and critique of these experiments. This work was supported by NIH/NEI U01 EY027266 and U24 EY029890 as well as the Department of Defense through the Vision Research Program under award no. W81XWH-20-1-0655. Opinions, interpretations, conclusions, and recommendations are those of the authors and are not necessarily endorsed by the Department of Defense. This work was also supported by Fighting Blindness Canada (including philanthropic support from Donna Green and Goldie Feldman), Research to Prevent Blindness, Retina Research Foundation Emmett A. Humble Distinguished Directorship, McPherson ERI Sandra Lemke Trout Chair in Eye Research, philanthropic support from Arthur and Nancy Nesbitt (D.M.G.), NIH/MH116582 (X.Z.), and NIH/NICHD U54HD090256 and P50HD105353. A.L.L. was supported by the UW SVM Dean's office, NIH/NEI U24 EY029890, and NIH/NEI F30 EY031230. S.J.M. was supported by a UW-Madison Stem Cell and Regenerative Medicine Center training grant and the Foundation Fighting Blindness.

Author affiliations: [a]Comparative Biomedical Sciences Graduate Program, University of Wisconsin–Madison, Madison, WI 53705; [b]Waisman Center, University of Wisconsin–Madison, Madison, WI 53705; [c]McPherson Eye Research Institute, University of Wisconsin–Madison, Madison, WI 53705; [d]Cellular and Molecular Pathology Graduate Program, University of Wisconsin–Madison, Madison, WI 53705; [e]Department of Neuroscience, University of Wisconsin–Madison, Madison, WI 53705; and [f]Department of Ophthalmology and Visual Sciences, University of Wisconsin–Madison, Madison, WI 53705

Author contributions: A.L.L., S.J.M., X.Z., and D.M.G. designed research; A.L.L., S.J.M., C.B., and M.A.F.Z. performed research; Y.G., X.Z., and D.M.G. contributed new reagents/analytic tools; A.L.L., S.J.M., and M.B. analyzed data; and A.L.L., S.J.M., and D.M.G. wrote the paper.

Competing interest statement: The authors declare competing interests and have patent filings to disclose. D.M.G. has declared intellectual rights for production of 3D ROs through the Wisconsin Alumni Research Foundation, Madison, WI (US PTO No. 9,328,328). The authors have organizational affiliations and research support to disclose. D.M.G. has an ownership interest in and receives grant support from Opsis Therapeutics LLC, which has licensed the technology to generate ROs from hPSCs utilized in this publication. The terms of this arrangement have been reviewed and approved by the University of Wisconsin-Madison in accordance with its conflict-of-interest policies. All other authors declare no competing interests.

1. S. R. y. Cajal, Estructura de los centros nerviosos de las aves. *Revista Trimestral de Histología Normal y Patológica,* **1**, 1–10 (1888).
2. F. Soto, D. Kerschensteiner, Synaptic remodeling of neuronal circuits in early retinal degeneration. *Front. Cell. Neurosci.* **9**, 395 (2015).
3. B. W. Jones, R. E. Marc, Retinal remodeling during retinal degeneration. *Exp. Eye Res.* **81**, 123–137 (2005).
4. H. A. Quigley, Glaucoma. *Lancet* **377**, 1367–1377 (2011).
5. J. Ribeiro *et al.*, Restoration of visual function in advanced disease after transplantation of purified human pluripotent stem cell-derived cone photoreceptors. *Cell Rep.* **35**, 109022 (2021).
6. S. J. Gasparini, S. Llonch, O. Borsch, M. Ader, Transplantation of photoreceptors into the degenerative retina: Current state and future perspectives. *Prog. Retin. Eye Res.* **69**, 1–37 (2018), 10.1016/j.preteyeres.2018.11.001.
7. A. L. Ludwig, D. M. Gamm, Outer retinal cell replacement: Putting the pieces together. *Transl. Vis. Sci. Technol.* **10**, 15 (2021).
8. K. Y. Zhang, E. A. Aguzzi, T. V. Johnson, Retinal ganglion cell transplantation: Approaches for overcoming challenges to functional integration. *Cells* **10**, 1426 (2021).
9. M. O. Karl, T. A. Reh, Regenerative medicine for retinal diseases: Activating endogenous repair mechanisms. *Trends Mol. Med.* **16**, 193–202 (2010).
10. J. Duebel, K. Marazova, J.-A. Sahel, Optogenetics. *Curr. Opin. Ophthalmol.* **26**, 226–232 (2015).
11. S. M.Becker, S. J. Tumminia, M. F. Chiang, The NEI Audacious Goals Initiative: Advancing the Frontier of Regenerative Medicine. *Trans. Vis. Sci. Tech.* **10**, 2–2 (2021).
12. C. Zhao, Q. Wang, S. Temple, Stem cell therapies for retinal diseases: Recapitulating development to replace degenerated cells. *Development* **144**, 1368–1381 (2017).
13. M. Garita-Hernandez *et al.*, Restoration of visual function by transplantation of optogenetically engineered photoreceptors. *Nat. Commun.* **10**, 4524 (2019).
14. E. Aboualizadeh *et al.*, Imaging transplanted photoreceptors in living nonhuman primates with single-cell resolution. *Stem Cell Rep.* **15**, 482–497 (2020).
15. A. O. Barnea-Cramer *et al.*, Function of human pluripotent stem cell-derived photoreceptor progenitors in blind mice. *Sci. Rep.* **6**, 29784 (2016).
16. G. Gagliardi *et al.*, Characterization and transplantation of CD73-positive photoreceptors isolated from human iPSC-derived retinal organoids. *Stem Cell Rep.* **11**, 665–680 (2018).
17. J. R. Chao *et al.*, Transplantation of human embryonic stem cell-derived retinal cells into the subretinal space of a non-human primate. *Transl. Vis. Sci. Technol.* **6**, 4 (2017).
18. S. Iraha *et al.*, Establishment of immunodeficient retinal degeneration model mice and functional maturation of human ESC-derived retinal sheets after transplantation. *Stem Cell Rep.* **10**, 1059–1074 (2018).
19. H.-Y. Tu *et al.*, Medium- to long-term survival and functional examination of human iPSC-derived retinas in rat and primate models of retinal degeneration. *EBioMedicine* **39**, 562–574 (2019).
20. B. T. McLelland *et al.*, Transplanted hESC-derived retina organoid sheets differentiate, integrate, and improve visual function in retinal degenerate rats. *Invest. Ophthalmol. Vis. Sci.* **59**, 2586–2603 (2018).
21. B. Lin *et al.*, Retina organoid transplants develop photoreceptors and improve visual function in RCS rats with RPE dysfunction. *Invest. Ophthalmol. Vis. Sci.* **61**, 34–34 (2020).
22. E. E. Capowski *et al.*, Reproducibility and staging of 3D human retinal organoids across multiple pluripotent stem cell lines. *Development* **146**, dev171686 (2019).
23. C. S. Cowan *et al.*, Cell types of the human retina and its organoids at single-cell resolution. *Cell* **182**, 1623–1640.e34 (2020).
24. C. M. Bell, D. J. Zack, C. A. Berlinicke, Human organoids for the study of retinal development and disease. *Annu. Rev. Vis. Sci.* **6**, 91–114 (2020).
25. M. J. Phillips *et al.*, Blood-derived human iPS cells generate optic vesicle-like structures with the capacity to form retinal laminae and develop synapsesproduction of retina from human blood iPS Cells. *Invest. Ophthalmol. Vis. Sci.* **53**, 2007–2019 (2012).
26. X. Zhong *et al.*, Generation of three-dimensional retinal tissue with functional photoreceptors from human iPSCs. *Nat. Commun.* **5**, 4047 (2014).
27. S. K. Ohlemacher *et al.*, "Advances in the differentiation of retinal ganglion cells from human pluripotent stem cells" in *Pluripotent Stem Cells in Eye Disease Therapy*, K. Bharti, Ed. (Advances in Experimental Medicine and Biology, Springer International Publishing, 2019), vol. **1186**, pp. 121–140.
28. D. Hallam *et al.*, Human-induced pluripotent stem cells generate light responsive retinal organoids with variable and nutrient-dependent efficiency. *Stem Cells* **36**, 1535–1551 (2018).
29. S. Kim *et al.*, Generation, transcriptome profiling, and functional validation of cone-rich human retinal organoids. *Proc. Natl. Acad. Sci. U.S.A.* **116**, 10824–10833 (2019).
30. S. K. Rempel *et al.*, Human photoreceptors switch from autonomous axon extension to cell-mediated process pulling during synaptic marker redistribution. *Cell Rep.* **39**, 110827 (2022).
31. A. Saha *et al.*, Cone photoreceptors in human stem cell-derived retinal organoids demonstrate intrinsic light responses that mimic those of primate fovea. *Cell Stem Cell* **29**, 460–471.e3 (2022).
32. M. J. Phillips *et al.*, A novel approach to single cell RNA-Sequence analysis facilitates in silico gene reporting of human pluripotent stem cell-derived retinal cell types. *Stem Cells* **36**, 313–324 (2018).
33. A. Kallman *et al.*, Investigating cone photoreceptor development using patient-derived NRL null retinal organoids. *Commun. Biol.* **3**, 82 (2020).
34. Y.-P. Yang *et al.*, Glutamate stimulation dysregulates AMPA receptors-induced signal transduction pathway in Leber's inherited optic neuropathy patient-specific hiPSC-derived retinal ganglion cells. *Cells* **8**, 625 (2019).
35. K. B. Langer *et al.*, Retinal ganglion cell diversity and subtype specification from human pluripotent stem cells. *Stem Cell Rep.* **10**, 1282–1293 (2018).
36. V. Cora *et al.*, A cleared view on retinal organoids. *Cells* **8**, 391 (2019).
37. A. Gonzalez-Cordero *et al.*, Recapitulation of human retinal development from human pluripotent stem cells generates transplantable populations of cone photoreceptors. *Stem Cell Rep.* **9**, 820–837 (2017).
38. K. J. Wahlin *et al.*, Photoreceptor outer segment-like structures in long-term 3D retinas from human pluripotent stem cells. *Sci. Rep.* **7**, 766 (2017).
39. R. K. Singh *et al.*, Characterization of three-dimensional retinal tissue derived from human embryonic stem cells in adherent monolayer cultures. *Stem Cells Dev.* **24**, 2778–2795 (2015).
40. K. B. VanderWall *et al.*, Astrocytes regulate the development and maturation of retinal ganglion cells derived from human pluripotent stem cells. *Stem Cell Rep.* **12**, 201–212 (2019).
41. A. O. Barnea-Cramer *et al.*, Repair of retinal degeneration following ex vivo minicircle DNA gene therapy and transplantation of corrected photoreceptor progenitors. *Mol. Therapy* **28**, 830–844 (2020).
42. D. Zerti *et al.*, Transplanted pluripotent stem cell-derived photoreceptor precursors elicit conventional and unusual light responses in mice with advanced retinal degeneration. *Stem Cells* 882–896 (2021), 10.1002/stem.3365.
43. M. Mandai *et al.*, iPSC-derived retina transplants improve vision in rd1 end-stage retinal-degeneration mice. *Stem Cell Rep.* **8**, 69–83 (2017).
44. T. Léveillard, L. Klipfel, Mechanisms underlying the visual benefit of cell transplantation for the treatment of retinal degenerations. *Int. J. Mol. Sci.* **20**, 557 (2019).
45. P. E. B. Nickerson, A. Ortin-Martinez, V. A. Wallace, Material exchange in photoreceptor transplantation: Updating our understanding of donor/host communication and the future of cell engraftment science. *Front. Neural Circuits* **12**, 17 (2018).
46. C. Saleeba, B. Dempsey, S. Le, A. Goodchild, S. McMullan, A student's guide to neural circuit tracing. *Front. Neurosci.* **13** (2019).
47. A. Rogers, K. T. Beier, Can transsynaptic viral strategies be used to reveal functional aspects of neural circuitry? *J. Neurosci. Methods* **348**, 109005 (2021).
48. I. R. Wickersham *et al.*, Monosynaptic restriction of transsynaptic tracing from single, genetically targeted neurons. *Neuron* **53**, 639–647 (2007).
49. E. M. Callaway, L. Luo, Monosynaptic circuit tracing with glycoprotein-deleted rabies viruses. *J. Neurosci.* **35**, 8979–8985 (2015).
50. A. F. Adler, A. Björklund, M. Parmar, Transsynaptic tracing and its emerging use to assess graft-reconstructed neural circuits. *Stem Cells* **38**, 716–726 (2020).
51. S. Palma-Tortosa, B. Coll-San Martin, Z. Kokaia, D. Tornero, Neuronal replacement in stem cell therapy for stroke: Filling the gap. *Front. Cell Dev. Biol.* (2021).
52. M. Grønning Hansen *et al.*, Grafted human pluripotent stem cell-derived cortical neurons integrate into adult human cortical neural circuitry. *Stem Cells Transl. Med.* **9**, 1365–1377 (2020).

53. C. Gomes *et al.*, Astrocytes modulate neurodegenerative phenotypes associated with glaucoma in OPTN(E50K) human stem cell-derived retinal ganglion cells. *Stem Cell Rep.* **17**, 1636–1649 (2022).
54. C. M. Fligor *et al.*, Extension of retinofugal projections in an assembled model of human pluripotent stem cell-derived organoids. *Stem Cell Rep.* **16**, 2228–2241 (2021).
55. J. A. Thomson *et al.*, Embryonic stem cell lines derived from human blastocysts. *Science* **282**, 1145–1147 (1998).
56. K. H. Pfenninger, The cytochemistry of synaptic densities. II. Proteinaceous components and mechanism of synaptic connectivity. *J. Ultrastruct. Res.* **35**, 451–475 (1971).
57. J. E. Huettner, R. W. Baughman, Primary culture of identified neurons from the visual cortex of postnatal rats. *J. Neurosci.* **6**, 3044–3060 (1986).
58. L. Sun *et al.*, Differences in neurotropism and neurotoxicity among retrograde viral tracers. *Mol. Neurodegener.* **14**, 8 (2019).
59. Y. Feodorova, M. Koch, S. Bultman, S. Michalakis, I. Solovei, Quick and reliable method for retina dissociation and separation of rod photoreceptor perikarya from adult mice. *MethodsX* **2**, 39–46 (2015).
60. K. Kruczek, A. Swaroop, Pluripotent stem cell-derived retinal organoids for disease modeling and development of therapies. *Stem Cells* **38**, 1206–1215 (2020).
61. M. J. Phillips *et al.*, Generation of a rod-specific NRL reporter line in human pluripotent stem cells. *Sci. Rep.* **8**, 2370 (2018).
62. I.-K. Lee *et al.*, Ultrathin micromolded 3D scaffolds for high-density photoreceptor layer reconstruction. *Sci. Adv.* **7**, eabf0344 (2021).
63. R. Schniepp *et al.*, Retinal colocalization and in vitro interaction of the glutamate receptor EAAT3 and the serum- and glucocorticoid-inducible kinase SGK1. *Invest. Ophthalmol. Vis. Sci.* **45**, 1442–1449 (2004).
64. Y. Sun *et al.*, Loss of MeCP2 in immature neurons leads to impaired network integration. *Hum. Mol. Genet.* **28**, 245–257 (2019).
65. W. Guo *et al.*, Fragile X proteins FMRP and FXR2P control synaptic GluA1 expression and neuronal maturation via distinct mechanisms. *Cell Rep.* **11**, 1651–1666 (2015).
66. Y. Gao *et al.*, RGS6 mediates effects of voluntary running on adult hippocampal neurogenesis. *Cell Rep.* **32**, 107997 (2020).
67. C. Vivar *et al.*, Monosynaptic inputs to new neurons in the dentate gyrus. *Nat. Commun.* **3**, 1107 (2012).
68. T. K. Lavin, L. Jin, N. E. Lea, I. R. Wickersham, Monosynaptic tracing success depends critically on helper virus concentrations. *Front. Synaptic Neurosci.* **12**, 6 (2020).
69. A. Ortin-Martinez *et al.*, A reinterpretation of cell transplantation: GFP Transfer from donor to host photoreceptors. *Stem Cells* **35**, 932–939 (2017).
70. R. A. Pearson *et al.*, Donor and host photoreceptors engage in material transfer following transplantation of post-mitotic photoreceptor precursors. *Nat. Commun.* **7**, 13029 (2016).
71. T. Santos-Ferreira *et al.*, Retinal transplantation of photoreceptors results in donor-host cytoplasmic exchange. *Nat. Commun.* **7**, 13028 (2016).
72. M. S. Singh *et al.*, Transplanted photoreceptor precursors transfer proteins to host photoreceptors by a mechanism of cytoplasmic fusion. *Nat. Commun.* **7**, 13537 (2016).
73. S. Decembrini *et al.*, Cone genesis tracing by the Chrnb4-EGFP mouse line: Evidences of cellular material fusion after cone precursor transplantation. *Mol. Ther.* **25**, 634–653 (2017).
74. M. S. Singh *et al.*, Retinal stem cell transplantation: Balancing safety and potential. *Prog. Retin. Eye Res.* **75**, 100779 (2020).
75. Y. Wang, D. Zhang, B. Shen, Y. Zhang, P. Gu, Stem/progenitor cells and biodegradable scaffolds in the treatment of retinal degenerative diseases. *Curr. Stem Cell Res. Ther.* **13**, 160–173 (2018).
76. J. Assawachananont *et al.*, Transplantation of embryonic and induced pluripotent stem cell-derived 3D retinal sheets into retinal degenerative mice. *Stem Cell Rep.* **2**, 662–674 (2014).
77. A. T. Foik *et al.*, Detailed visual cortical responses generated by retinal sheet transplants in rats with severe retinal degeneration. *J. Neurosci.* **38**, 10709–10724 (2018).
78. S. B. Rompani *et al.*, Different modes of visual integration in the lateral geniculate nucleus revealed by single-cell-initiated transsynaptic tracing. *Neuron* **93**, 767–776.e6 (2017).
79. S. Camelo, J. Castellanos, M. Lafage, M. Lafon, Rabies virus ocular disease: T-cell-dependent protection is under the control of signaling by the p55 tumor necrosis factor alpha receptor, p55TNFR. *J. Virol.* **75**, 3427–3434 (2001).
80. C. R. J. Laver, J. A. Matsubara, Structural divergence of essential triad ribbon synapse proteins among placental mammals – Implications for preclinical trials in photoreceptor transplantation therapy. *Exp. Eye Res.* **159**, 156–167 (2017).
81. A. Ludwig, hPSC-derived Photoreceptor Synaptic Puncta and Synaptic Tracing Datasets and Code. Mendeley Data. 10.17632/ncmn2msdhx. Deposited 20 December 2022.